Analysis of Millimeter Waveguides on Anisotropic Substrates Using the Three-Dimensional Transmission-Line Matrix Method

Ceyhun Bulutay, *Student Member, IEEE* and Sheila Prasad, *Senior Member, IEEE*

Abstract— **Three-dimensional condensed asymmetrical node, variable grid, transmission-line matrix (TLM) method has been used in analyzing several millimeter waveguides on anisotropic substrates. The dispersion characteristics of image guides together with field and energy confinement properties at millimeter-wave frequencies have been investigated. Edge coupled microstrip line on a uniaxial substrate is analyzed for the even and odd mode dispersion characteristics. Finally the same analysis is repeated for bilateral fin lines on uniaxial/biaxial substrates. The results obtained using other computational techniques are included in all of these cases to assess the competence of the method.**

I. Introduction

AT MILLIMETER-WAVE frequencies, planar guided wave structures have proven their superiority with their inherent compatibility with microwave electronic circuitry. These promising transmission lines can be classified as [1]: Planar and quasi-planar lines (microstrip like transmission lines, fin lines), dielectric guides (dielectric slab, image line, insular guide etc.), H-guides (groove guide, through guide etc.). Most of these planar transmission lines cannot be treated analytically other than with oversimplified conditions. On the other hand, several computational techniques have been successfully applied to the exploration of these structures [2].

In this paper, the three-dimensional, asymmetrical condensed node variable grid transmission line matrix (TLM) method has been developed as a tool for analyzing millimeter waveguides (possibly on anisotropic substrates). Due to its time domain formulation, TLM is free from costly matrix operations such as matrix inversion or eigenvalue computation. Moreover, it is superior to other time domain methods such as the finite-difference time-domain technique that is limited by a Courant stability criterion whereas the TLM is inherently stable due to its physical foundation [3]. The most appealing feature of TLM for millimeter-wave engineering is the wide variety of geometries that can be examined without requiring any reformulation. In particular, metallic strips and symmetry planes cause no modification in the algorithm and are welcomed by the method.

Manuscript received May 21, 1992; revised October 23, 1992.

C. Bulutay was and S. Prasad is with the Department of Electrical and Computer Engineering, Northeastern University, Boston, MA 02115. C. Bulutay is now with the Electrical and Electronic Engineering Department, Middle East Technical University, Ankara 06531, Turkey.

IEEE Log Number 9209332.

It is to be noted that H-guides are not treated in this paper since they are not compatible with microwave integrated circuits. However, the field and energy confinement as well as dispersion characteristics of image guides are investigated in detail. The ability of the TLM to accommodate anisotropic media has been utilized in the investigation of the dispersive behaviour of edge coupled microstrip lines on a uniaxial substrate. The more general case of biaxial substrates have been treated together with uniaxial ones for the bilateral fin lines. The results obtained using other computational techniques are also included in all of these cases providing an objective comparison to prove the validity of this work.

II. Three Dimensional Transmission Line Matrix Method

Although the physical basis of TLM lies in Huygen's principle of wave propagation [3], the underlying mathematical concept of transmission line modelling can be illustrated as shown in Fig. 1.

The voltages and currents in the transmission line lattice have to simulate the actual physical variables everywhere over the computation domain. For this reason it may be appropriate to rename the technique "TLM—The Equation Simulator."

Maxwell's equations in their differential form are point relations whereas both the finite-difference time-domain and the expanded node TLM method cannot allocate all six components of the fields to a single point in space. This can cause errors in defining the position of the boundaries and dielectric layers. Vital quantities such as Poynting's vector cannot be represented accurately. For these reasons the condensed node schemes that have been recently proposed are of primary importance [4], [5]. The asymmetrical version of the condensed node TLM has been preferred in this work for which the final form of the equivalent circuit is shown in Fig. 2. It possesses

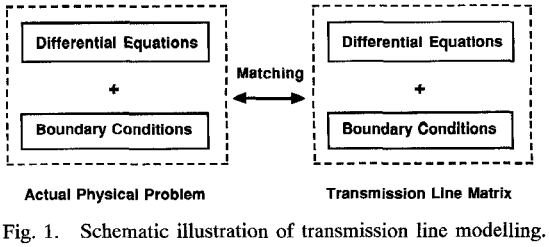

Fig. 1. Schematic illustration of transmission line modelling.

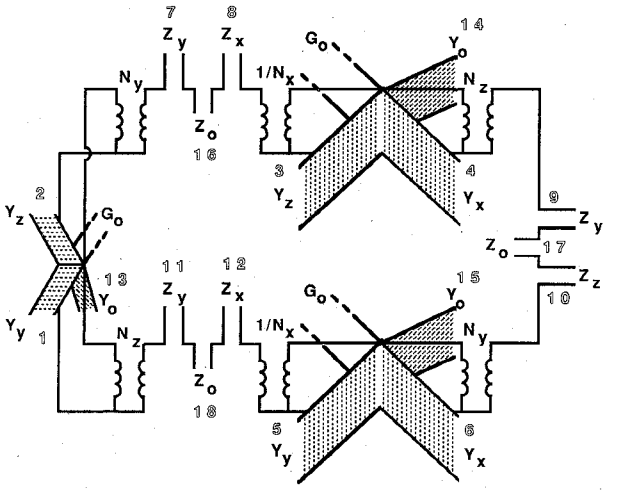

Fig. 2. Lumped equivalent circuit of an asymmetrical condensed node.

the additional feature of variable grid size and is essentially an 18 port circuit. The lengths of the connecting link lines that also manifest the variable grid formulation are indicated in Fig. 3. The characteristic admittances at the shunt nodes and the characteristic impedances at the series connected nodes must satisfy the following relations:

$$Y_x = Y_0/N_{x1}, \qquad Y_y = Y_0/N_{yb}, \qquad Y_z = Y_0/N_{zf} \quad (1)$$

$$Z_x = Z_0/N_{xr}, \qquad Z_y = Z_0/N_{yu}, \qquad Z_z = Z_0/N_{zb} \quad (2)$$

In order to satisfy Maxwell's two curl equations, the transformer ratios in Fig. 2 must be determined from the following equations.

$$N_x = \sqrt{N_{x1}N_{xr}}, \qquad N_y = \sqrt{N_{yu}N_{yb}}, \qquad N_z = \sqrt{N_{zf}N_{zb}} \quad (3)$$

The classical foundations of the TLM method can be found in several well written papers such as [6] and will not be given in this paper. However, the final set of equations used in this work for a general anisotropic medium can be listed.

$$Y_x = Y_0/N_x, \qquad Y_y = Y_0/N_y, \qquad Y_z = Y_0/N_z \quad (4)$$

$$Z_x = Z_0/N_x, \qquad Z_y = Z_0/N_y, \qquad Z_z = Z_0/N_z \quad (5)$$

$$Y_{t1} = Y_{dx} + G_{0x} + Y_y + Y_z$$

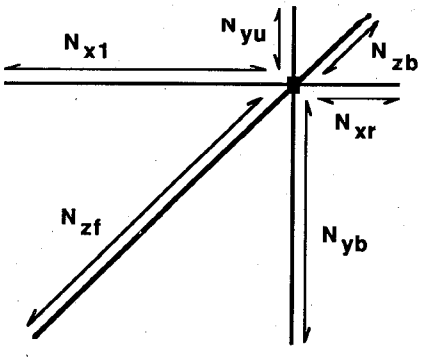

Fig. 3. The link lines associated with a general variable grid condensed node.

where

$$Y_{di} = Y_0 4(\varepsilon_{ri} - 1) \quad (6)$$

$$Y_{t2} = Y_{dy} + G_{0y} + Y_z + Y_x$$

where

$$G_{0i} = Y_0 \sigma_i Z_{air}\, \Delta 1 \quad (7)$$

$$Y_{t3} = Y_{dz} + G_{0z} + Y_y + Y_x$$

where

$$Z_{mi} = Z_0 4(\mu_{ri} - 1) \quad (8)$$

$$Z_{t1} = Z_{mz} + Z_y + Z_x \quad (9)$$

$$Z_{t2} = Z_{mx} + Z_y + Z_z \quad (10)$$

$$Z_{t3} = Z_{my} + Z_z + Z_x \quad (11)$$

$$N_1 = N_y, \qquad N_2 = N_z, \qquad N_3 = N_x \quad (12)$$

$$D_i = Z_{tj} + 1/\left(N_i^2 Y_{tk}\right) + 1/\left(N_j^2 Y_{tj}\right) \quad (13)$$

$$Y_{ci} = Y_{tk} Y_{tj} D_i N_i^2 N_j^2 \quad (14)$$

$$Z_{ai} = Z_{tk}(N_k/N_i)^2 + Z_{tj}/\left(N_i^2 D_i Y_{tk}\right) \quad (15)$$

$$Z_{bi} = Z_{ti}(N_k/N_j)^2 + Z_{tj}/\left(N_j^2 D_i Y_{tj}\right) \quad (16)$$

$$Y_{eqi} = (N_k/(N_j N_i))^2 \cdot (Y_{ci}(Z_{ai} + Z_{bi})/(Y_{ci} Z_{ai} Z_{bi} + Z_{ai} + Z_{bi})) \quad (17)$$

$$D_1' = Y_{tk} + 1/\left(N_i^2 Z_{tj}\right) + 1/\left(N_k^2 Z_{tk}\right) \quad (18)$$

$$Z_{ci} = Z_{tk} Z_{tj} D_i' N_k^2 N_i^2 \quad (19)$$

$$Y_{ai} = Y_{ti}(N_j/N_k)^2 + Y_{tk}/\left(N_k^2 D_i' Z_{tk}\right) \quad (20)$$

$$Y_{bi} = Y_{tj}(N_j/N_i)^2 + Y_{tk}/\left(N_i^2 D_i' Z_{tj}\right) \quad (21)$$

$$Z_{eqi} = (N_j/(N_i N_k))^2 \cdot (Z_{ci}(Y_{ai} + Y_{bi})/(Z_{ci} Y_{ai} Y_{bi} + Y_{ai} + Y_{bi})) \quad (22)$$

$$Z_{vi} = 2/(Y_{ti} + Y_{eqi}) \quad (23)$$

$$Y_{vi} = 2/(Z_{eqi} + Z_{ti}) \quad (24)$$

$$a_i = Z_{vi} \quad (25)$$

$$b_i = Z_{vi}(N_k/N_i)\left(1 - Y_{eqi} N_i^2 Z_{ti} Z_{ai}\right)/(Z_{ai} + Z_{bi})) \quad (26)$$

$$c_i = (N_k/N_j) Z_{vi}\left(1 - Y_{eqi} Z_{tk} N_j^2 Z_{bi}/(Z_{ai} + Z_{bi})\right) \quad (27)$$

$$d_i = Z_{vi} Y_{eqi} N_j Z_{ai}/(Z_{ai} + Z_{bi}) \quad (28)$$

$$f_i = Z_{vi}Y_{eqi}N_jZ_{bi}/(Z_{ai}+Z_{bi}) \quad (29)$$

$$e_i = (c_i/N_i - b_i/N_j)/Z_{tj} \quad (30)$$

$$j_i = Y_{vi} \quad (31)$$

$$k_i = Y_{vi}(N_j/N_k)\big(1 - Z_{eqi}N_k^2Y_{tj}Y_{ai}/(Y_{ai}+Y_{bi})\big) \quad (32)$$

$$1_i = (N_j/N_i)Y_{vi}\big(1 - Z_{eqi}Y_{ti}N_i^2Y_{bi}/(Y_{ai}+Y_{bi})\big) \quad (33)$$

$$g_i = Y_{vi}Z_{eqi}N_iY_{bi}/(Y_{ai}+Y_{bi}) \quad (34)$$

$$h_i = Y_{vi}Z_{eqi}N_kY_{ai}/(Y_{ai}+Y_{bi}) \quad (35)$$

$$i_i = (1_i/N_k - k_i/N_i)/Y_{tk} \quad (36)$$

where the indices i, j, k have to be changed as for

$$i = 1, \quad j = 2 \quad \text{and} \quad k = 3$$

for

$$i = 2, \quad j = 3 \quad \text{and} \quad k = 1$$

and for

$$i = 3, \quad j = 1 \quad \text{and} \quad k = 2.$$

With these equations the compact representation of the 18×18 scattering matrix is given as in [4]:

In using the matrix, the Y values over the first row multiply the corresponding columns, similarly the Z values to left of the first column also multiply the related rows and hence, say, $S_{7,i} = Z_y d_i Y_Y$. It must be further pointed out that when the total voltages and currents are used instead of the incident and reflected voltage waves, the need for the above 18×18 matrix is avoided. Another advantage of this formulation is the ultimate need for the total voltages and currents since they are the quantities equivalent to the fields E and H. The reflected waves can in turn be obtained from the total and incident voltages. This allows a three times reduction both in size and the overall computation time.

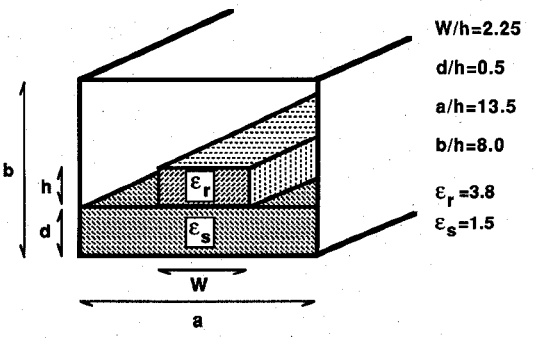

Fig. 4. Insulated image guide structure.

III. Analysis of Planar Millimeter Waveguides

A. Insulated Image Guide

The insulated image guide traps most of the energy inside the upper rectangular dielectric away from the conducting ground plane when $\epsilon_r > \epsilon_s$, in effect decreasing the conductor losses which cause problems at millimeter-wave frequencies. The geometry and the physical dimensions of the shielded image guide used in this work are given in Fig. 4.

A magnetic wall has been used in the implementation due to the symmetry of the structure. Fig. 5 shows the dispersion characteristics of the E_y^{11} mode and also compares the results with the finite difference method [7] that was specifically devised for these applications. The deviation in the high end of hk_o is due to the dispersion degradation of the TLM method and it can be avoided by decreasing the unit mesh length. Such an adjustment was done at $hk_o = 1.75$ which resulted in perfect agreement between the two results. About the discrepancy around $hk_o = 1.5$ see the discussions and conclusion section.

Different field plots have been generated to investigate the physics behind the wave guiding phenomenon (Fig. 6–9). Strictly speaking these are the transverse field distributions of an insulated image guide based cavity. An equal grid prototype of the structure had to be developed for the correct 3-D representation of the distribution. Due to the relatively coarse

		1	2	3	4	5	6	7	8	9	10	11	12	13	14	15	16	17	18
		Y_y	Y_z	Y_z	Y_x	Y_x	Y_y							Y_{dx}	Y_{dy}	Y_{dz}			
1		a_1-1	a_1	c_2	c_2	b_3	b_3	g_1	$-g_1$	i_2	$-l_2$	h_3	$-h_3$	a_1	c_2	b_3	$-g_1$	$-i_2$	$-h_3$
2		a_1	a_1-1	c_2	c_2	b_3	b_3	g_1	$-g_1$	i_2	$-i_2$	h_3	$-h_3$	a_1	c_2	b_3	$-g_1$	$-i_2$	$-h_3$
3		b_1	b_1	a_2-1	a_2	c_3	c_3	$-h_1$	h_1	$-g_2$	g_2	$-i_3$	i_3	b_1	a_2	c_3	h_1	g_2	i_3
4		b_1	b_1	a_2	a_2-1	c_3	c_3	$-h_1$	h_1	$-g_2$	g_2	$-i_3$	i_3	b_1	a_2	c_3	h_1	g_2	i_3
5		c_1	c_1	b_2	b_2	a_3-1	a_3	i_1	$-i_1$	h_2	$-h_2$	$-g_3$	g_3	c_1	b_2	a_3	$-i_1$	$-h_2$	$-g_3$
6		c_1	c_1	b_2	b_2	a_3	a_3-1	i_1	$-i_1$	h_2	$-h_2$	$-g_3$	g_3	c_1	b_2	a_3	$-i_1$	$-h_2$	$-g_3$
7	Z_Y	d_1	d_1	$-f_2$	$-f_2$	e_3	e_3	$1-j_1$	j_1	l_2	$-l_2$	k_3	$-k_3$	d_1	$-f_2$	e_3	j_1	$-l_2$	$-k_3$
8	Z_X	$-d_1$	$-d_1$	f_2	f_2	$-e_3$	$-e_3$	j_1	$1-j_1$	$-l_2$	l_2	$-k_3$	k_3	$-d_1$	f_2	$-e_3$	$-j_1$	l_2	k_3
9	Z_Y	e_1	e_1	$-d_2$	$-d_2$	f_3	f_3	k_1	$-k_1$	$1-j_2$	j_2	$-l_3$	l_3	e_1	$-d_2$	f_3	$-k_1$	j_2	l_3
10	ZZ	$-e_1$	$-e_1$	d_2	d_2	$-f_3$	$-f_3$	$-k_1$	k_1	j_2	$1-j_2$	l_3	$-l_3$	$-e_1$	d_2	$-f_3$	k_1	$-j_2$	$-l_3$
11	Z_Z	f_1	f_1	$-e_2$	$-e_2$	$-d_3$	$-d_3$	l_1	$-l_1$	$-k_2$	k_2	$1-j_3$	j_3	f_1	$-e_2$	$-d_3$	$-l_1$	k_2	j_3
12	Z_X	$-f_1$	$-f_1$	e_2	e_2	d_3	d_3	-1_1	l_1	k_2	$-k_2$	j_3	$1-j_3$	$-f_1$	e_2	d_3	l_1	$-k_2$	$-j_3$
13		a_1	a_1	c_2	c_2	b_3	b_3	g_1	$-g_1$	i_2	$-i_2$	h_3	$-h_3$	a_1-1	c_2	b_3	$-g_1$	$-i_2$	$-h_3$
14		b_1	b_1	a_2	a_2	c_3	c_3	$-h_1$	h_1	$-g_2$	g_2	$-i_3$	i_3	b_1	a_2-1	c_3	h_1	g_2	i_3
15		c_1	c_1	b_2	b_2	a_3	a_3	i_1	$-i_1$	h_2	$-h_2$	$-g_3$	g_3	c_1	b_2	a_3-1	$-i_1$	$-h_2$	$-g_3$
16	Z_{mz}	$-d_1$	$-d_1$	f_2	f_2	$-e_3$	$-e_3$	j_1	$-j_1$	$-l_2$	l_2	$-k_3$	k_3	$-d_1$	f_2	$-e_3$	$1-j_1$	l_2	k_3
17	Z_{mx}	$-e_1$	$-e_1$	d_2	d_2	$-f_3$	$-f_3$	$-k_1$	k_1	j_2	$-j_2$	l_3	$-l_3$	$-e_1$	d_2	$-f_3$	k_1	$1-j_2$	$-l_3$
18	Z_{my}	$-f_1$	$-f_1$	e_2	e_2	d_3	d_3	$-l_1$	l_1	k_2	$-k_2$	j_3	$-j_3$	$-f_1$	e_2	d_3	l_1	$-k_2$	$1-j_3$

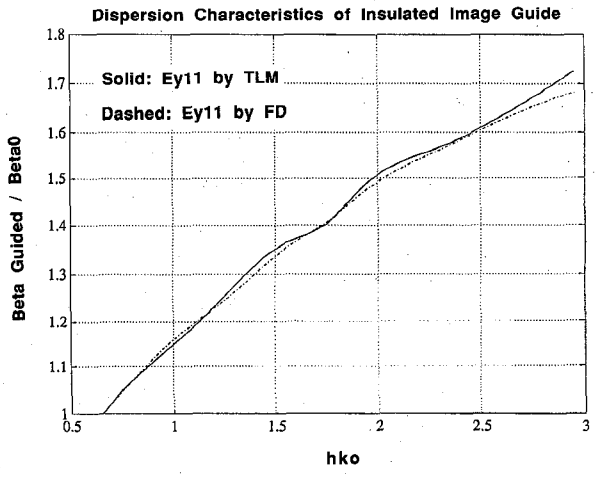

Fig. 5. E_y^{11} mode dispersion characteristics of insulated image guide. Solid line: TLM, Dashed line: Finite Difference [7].

mesh size the amplitude variations contain some marginal rapid variations. Eigenfrequencies have been chosen to be in the single moded region of the dispersion characteristics.

The effect of the upper dielectric is illustrated in Figs. 6 and 7 whereas Fig. 8 shows the E_x field distribution across the transverse plane. Finally, the energy density distribution

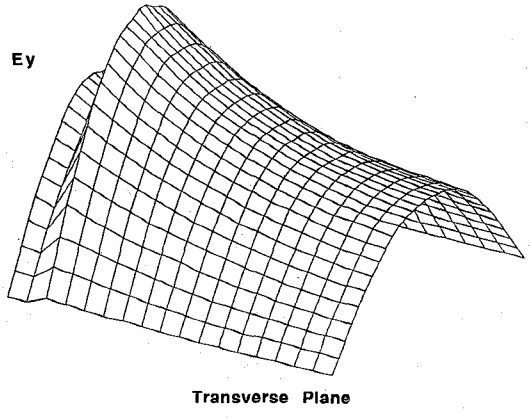

Fig. 6. E_y magnitude distribution over the transverse plane of the image guide (i.e. without the upper dielectric of the insulated image guide).

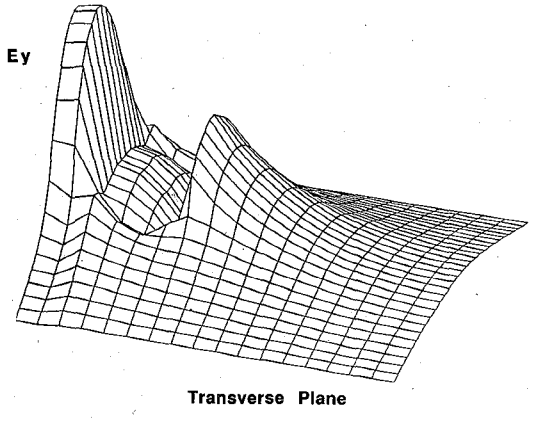

Fig. 7. E_y magnitude distribution over the transverse plane of the insulated image guide. Observe the effect of the upper rectangular dielectric when compared to Fig. 6.

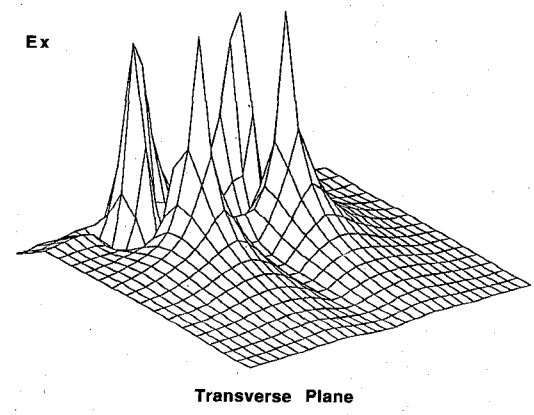

Fig. 8. E_x magnitude distribution over the transverse plane of the insulated image guide.

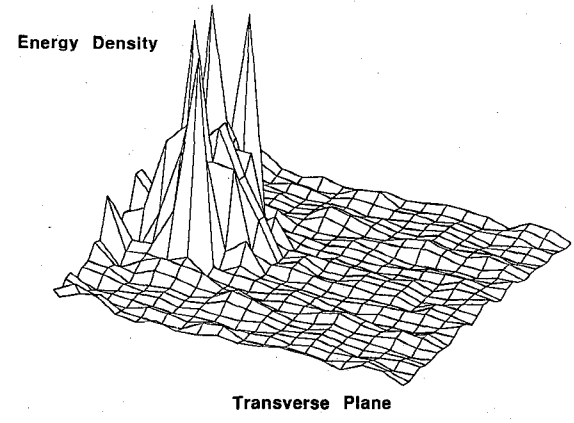

Fig. 9. Energy density distribution over the transverse plane of the insulated image guide.

on the transverse plane is shown in Fig. 9. It justifies the fact that the high permittivity slab guides most of the energy (away from the bottom conductor) according to design.

IV. Edge Coupled Microstrip Lines on Sapphire

Anisotropy has usually been considered to be undesirable, causing complexity in the theoretical formulation; however, most microwave substrates exhibit anisotropic behavior which is more pronounced at millimeter-wave frequencies. Moreover, it can have a significant advantage in the design of directional couplers. The main degradation for the directivity of a coupler has been found to be the unequal phase velocities of even and odd modes. Fortunately, the phase velocity equalization can be achieved by the use of anisotropic materials where a uniaxial material with higher permittivity is parallel to the ground rather than perpendicular to it [8].

With this motivation, the TLM method equipped with different perpendicular and parallel permittivity stubs is used for the analysis of the structure given in Fig. 10. The use of electric and magnetic walls for even and odd modes is illustrated in Fig. 11. The chosen grid size $\Delta l = 0.25$ mm corresponds to a time step of $\Delta t = \Delta l / c = 0.83$ ps. Fig. 12 and 13 show the dispersion characteristics of this structure obtained by TLM as well as those obtained by Fourier series techniques [9].

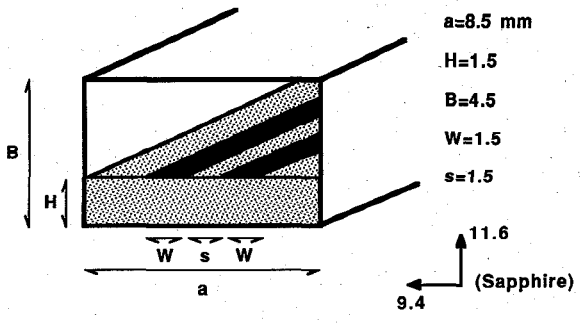

Fig. 10. Edge coupled microstrip lines on sapphire.

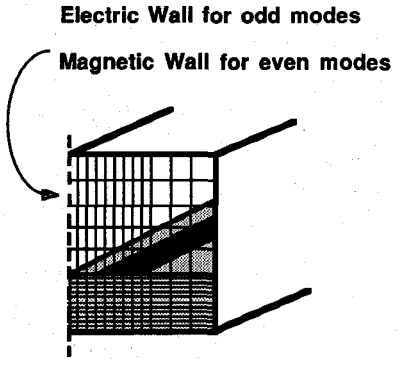

Fig. 11. The use of electric and magnetic symmetry planes for the even and odd mode analysis of edge coupled microstrip lines. Also the transverse variable grid allocation is illustrated but not drawn to scale.

V. Bilateral Fin Lines on Anisotropic Substrates

Bilateral fin lines on uniaxial and biaxial substrates have been analyzed using the tool that has been developed and compared with the published results of other full-wave techniques. The treatment, however, can be extended to all types of fin lines such as unilateral, insulated or antipodal fin lines without any difficulty since the metallizations have no effect on the form of the scattering matrices of the nodes.

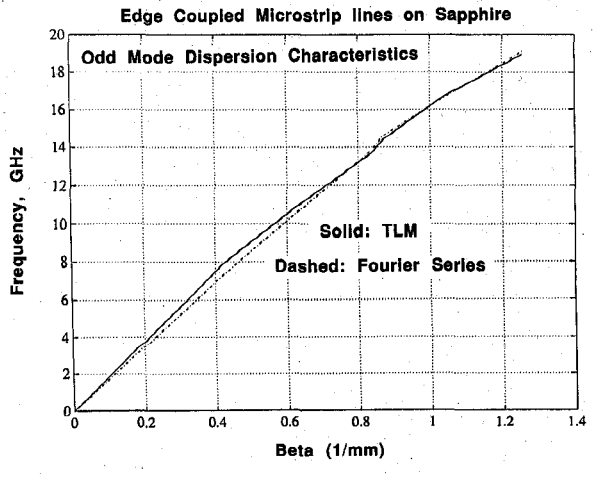

Fig. 12. Odd mode dispersion characteristics of edge coupled microstrip lines on sapphire. Solid line: TLM, dashed line: Fourier Series [9].

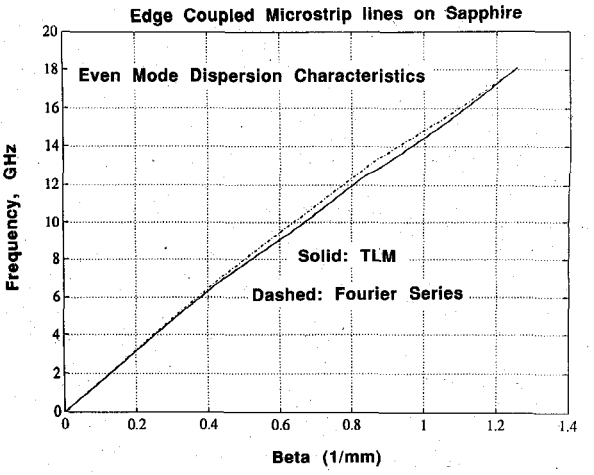

Fig. 13. Even mode dispersion characteristics of edge coupled microstrip lines on sapphire. Solid line: TLM, dashed line: Fourier Series [9].

A. Bilateral Fin line On Uniaxial Sapphire

A powerful technique based on the spectral domain procedure in conjunction with the Galerkin method has been used in [10] to obtain the characteristics of the fin lines. It is observed that, armed with the dominant mode excitation scheme, the TLM method can achieve these results with good accuracy. The physical dimensions of the bilateral fin line, embedded in WR-28 rectangular waveguide, are shown in Fig. 14(a). In addition, the placement of electric and magnetic walls as shown in Fig. 14(b) not only reduces the computational process but also favors the dominant mode excitation thereby resulting in fast convergence. The Δl value is chosen as 0.127 mm; however, due to the particular variable-grid formulation chosen to yield fast execution speed, an integer multiple of Δl must coincide with the physical dimensions, and thus, $d = 1.016$ mm $(= 8\Delta l)$ can be obtained instead of the actual value $d = 1.0$ mm.

The frequency dependent behavior of the effective permittivity is given in Fig. 15 as well as the results obtained in [10]. The permittivity values are extracted using $\epsilon_{eff} = (\beta_g/\beta_o)^2$. It is observed that the x and y components of the electric field just at the edge of the fin when excited in a standing wave distribution yield a good agreement with results reported in [10] even for small values of the observation period.

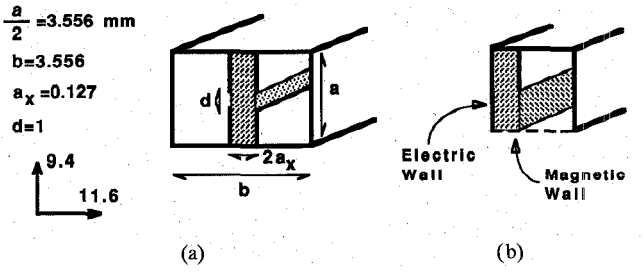

Fig. 14. (a) The geometry of the bilateral fin line on uniaxial sapphire. (b) The use of symmetry planes favoring dominant mode excitation and also yielding fast convergence.

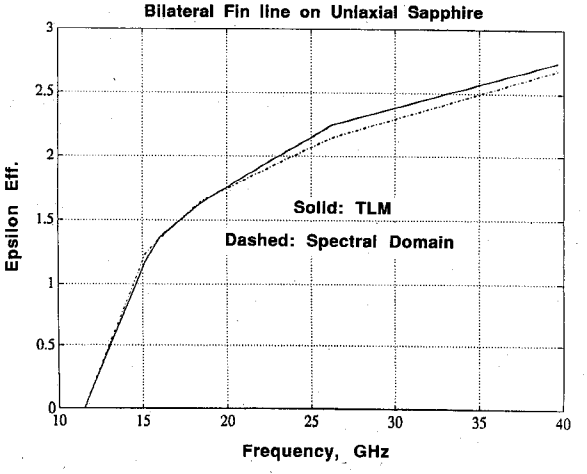

Fig. 15. Effective permittivity of the bilateral fin line on uniaxial sapphire. Solid line: TLM, dashed line: Spectral Domain [10].

B. Bilateral Fin Line On Biaxial PTFE

The TLM method described above can be applied to biaxial substrates without any additional cost. The dimensions are preserved to be the same as the previous case and sapphire is replaced by biaxial PTFE cloth (Fig. 16). The same boundary conditions as in Fig. 14(b) and the same excitation scheme is used. The results in Fig. 17 show good agreement with [10].

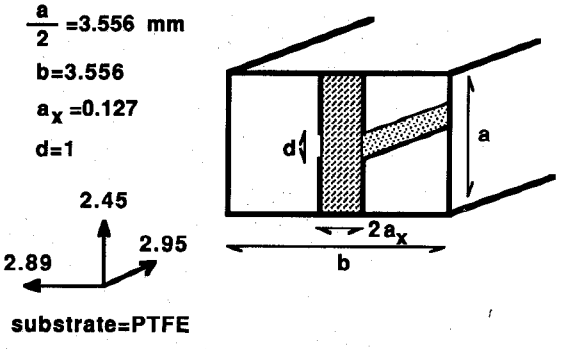

Fig. 16. The geometry of the bilateral fin line on biaxial PTFE cloth. (The dimensions are the same as those in Fig. 14(a)).

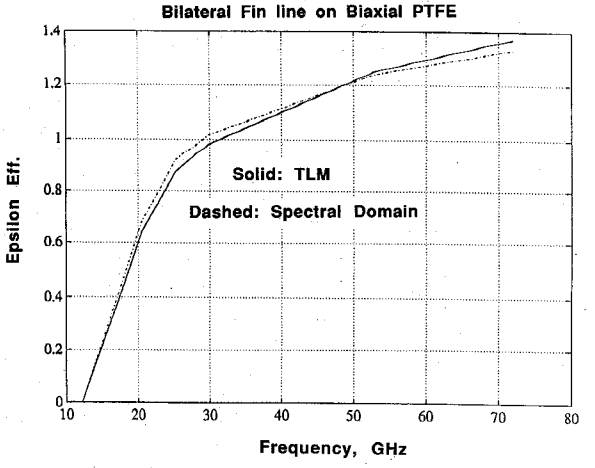

Fig. 17. Effective permittivity of the bilateral fin line on biaxial PTFE cloth. Solid line: TLM, dashed line: Spectral Domain [10].

VI. Discussions and Conclusion

Even though the physical phenomena must be the main purpose of a scientific work, the capabilities of the computational tools must also be well explored. In the quest for the solution of Maxwell's equations, it has been accepted that none of the techniques can be superior to the others in all aspects. The TLM method is no exception. So, it is in order, to caution about the usage of the technique in the characterization of millimeter waveguides. The primary output of any TLM application is a time waveform corresponding to the impulse response of the examined system. However, this time sequence can only be monitored for a finite time interval. In turn, its Fourier transform will not consist of a line spectrum (indicating the eigenfrequencies) but rather a superposition of $\sin(x)/x$ functions that may interfere with each other [6]. The error in the eigenfrequencies, associated to the finite observation window is inversely proportional to the distance between the two neighboring spectral peaks. In tracking the dispersion characteristics of a particular mode, a non-uniform convergence behavior is encountered depending on the contributions from the nearby modes. As a matter of fact, in the case of the insulated image guide considered in the previous section, the dispersion curves of the E_y^{11} mode and E_x^{11} mode intersect at $hk_o = 1.5$ [7]. In view of the above discussion, the deviation of the TLM solution around $hk_o = 1.5$ in Fig. 5 can be attributed to the strong overlap of these two modes. To avoid this problem the closeby modes must be suppressed while favoring the targetted mode by means of well chosen excitation scheme. Obviously, this necessitates some insight about the mode distribution. Alternatively, as a more systematic approach, the well developed signal processing techniques also offer remedial solutions to the truncation error and hence to non-uniform convergence. About this same problem, it has been claimed that for the Method of Lines (MoL), the optimum convergence is always assured if the strip edges contained in the structure are located in the right way between the discretization [11]. Thus nonscillating curves are expected from the MoL.

As mentioned previously, Finite Difference (in the frequency domain) and Spectral Domain Approach (SDA) have also been applied successfully to the millimeter waveguides. A common drawback of these two techniques as well as the MoL is that they lead to an eigenvalue equation or the computation of the zeros of a matrix. However, TLM is virtually free from any matrix operation due to its time domain formulation which circumvents the possible numerical instabilities. The memory requirement of TLM is larger than the other techniques due to the storage of the incident voltage waves filling all the computation space. However, this storage is static in the sense it is only for future usage not for any matrix operation. To give an idea, the structures considered in this paper have been analyzed with a memory requirement less than 3 Mbytes. An appreciable portion of the execution time is spent on the memory fetch cycles rather than arithmetic operations as in other techniques.

Other significant advantages of the TLM method are its versatility and inherent superiority in time domain problems.

However, in this work the frequency domain performance of the TLM is manifested in the analysis of millimeter-wave planar and quasi-planar waveguides taking into account anisotropy with no additional complexity. Among the different varieties of the guided structures analyzed, no change in the algorithm is needed due to the versatility of the method whereas in Spectral Domain Approach a lengthy and non-trivial analytical formulation is required for each structure. By the availability of wideband matched loads, the TLM will also have a potential application in linear/nonlinear microwave device characterization. With these features TLM will be a strong candidate as a general purpose, 3-D field based, microwave circuit simulator.

REFERENCES

[1] P. Bhartia and I. J. Bahl, *Millimeter Wave Engineering and Applications.* New York: Wiley, 1984.

[2] T. Itoh, Ed., *Numerical Techniques for Microwave and Millimeter-Wave Passive Structures.* New York: Wiley, 1989.

[3] P. B. Johns, "A new mathematical model to describe the physics of propagation," *Radio Electron. Eng.* vol. 44, pp. 657–666, Dec. 1974.

[4] P. Saguet, "The 3D Transmission-line matrix method: theory and comparison of the processes," *Int. J. Numer. Model.* vol. 2, pp. 191–200, 1989.

[5] P. B. Johns, "New symmetrical condensed node for three-dimensional solution of electromagnetic-wave problems by TLM," *Electron. Lett.,* vol. 22, pp. 162–164, Jan. 1986.

[6] W. J. R. Hoefer, "The transmission-line matrix (TLM) method," in *Numerical Techniques for Microwave and Millimeter-Wave Passive Structures,* ch. 8, T. Itoh, Ed., New York: Wiley, 1989, pp. 496–591.

[7] K. Bierwirth, N. Schulz and F. Arndt, "Finite-difference analysis of rectangular dielectric waveguide structures," *IEEE Trans. Microwave Theory Tech.,* vol. MTT-34, pp. 1104–1114, Nov. 1986.

[8] N. G. Alexopoulos and S. A. Maas, "Characteristics of microstrip directional couplers on anisotropic substrates," *IEEE Trans. Microwave Theory Tech.,* vol. MTT-30, pp. 1267–1270, Aug. 1982.

[9] N. G. Alexopoulos, "Integrated-circuit structures on anisotropic substrates," *IEEE Trans. Microwave Theory Tech.,* vol. MTT-33, pp. 847–881, Oct. 1985.

[10] H. Y. Yang, N. G. Alexopoulos, "Uniaxial and biaxial substrate effects on fin line characteristics," *IEEE Trans. Microwave Theory Tech.,* vol. MTT-35, pp. 24–29, Jan. 1987.

[11] U. Schulz, "On the edge condition with the method of lines in planar waveguides," *Arch. Elektron. Uebertragungstech.* vol. 34, pp. 176–178, 1980.

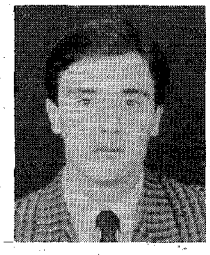

Ceyhun Bulutay (S'90) was born in Ankara, Turkey. He received his B.S. degree in electrical and electronic engineering from the Middle East Technical University, Ankara, Turkey in 1989. He has earned his M.S. degree on the area of fields, waves and optics in electrical and computer engineering from Northeastern University, Boston in 1991. Currently he is again in the electrical engineering department of Middle East Technical University studying for his Ph.D. degree.

From 1989 to 1991 he was a research assistant in Northeastern University working on microwave modelling of heterojunction bipolar transistors and computational electromagnetics. His current interests in METU are electromagnetics, ballistic electron transport and electron interference. Mr. Bulutay is a member of Eta Kappa Nu.

Sheila Prasad (M'80–SM'82) received the B. Sc. degree from the University of Mysore, India and the S.M. and Ph.D. degrees in Applied Physics from Harvard University. She has been on the faculty of the Department of Electrical Engineering at New Mexico State University, the Department of Materials Science and Engineering at the American University in Cairo, Egypt and the Department of Electrical and Electronics Engineering at the Birla Institute of Technology and Science, Pilani, India. She is presently a Professor in the Department of Electrical and Computer Engineering, Northeastern University, Boston, MA. Her areas of research interest include electromagnetics, microwave semiconductor devices and microwave solid state circuits.

Dr. Prasad is co-author with Prof. R. W. P. King of the book *Fundamental Electromagnetic Theory and Applications.* She is a member of Sigma Xi.